Acta Crystallographica Section D
Biological Crystallography
ISSN 0907-4449

Structure, recombinant expression and mutagenesis studies of the catalase with oxidase activity from *Scytalidium thermophilum*

Yonca Yuzugullu,[a] Chi H. Trinh,[b] Mark A. Smith,[c] Arwen R. Pearson,[b] Simon E. V. Phillips,[d] Didem Sutay Kocabas,[e] Ufuk Bakir,[f] Zumrut B. Ogel[g] and Michael J. McPherson[b]*

[a]Department of Biology, Kocaeli University, 41380 Kocaeli, Turkey, [b]Astbury Centre for Structural Molecular Biology, University of Leeds, Leeds LS2 9JT, England, [c]Université de Montréal, Montréal H3T 1J4, Canada, [d]Research Complex at Harwell, Rutherford Appleton Laboratory, Didcot OX11 0FA, England, [e]Food Engineering Department, Karamanoğlu Mehmetbey University, 70200 Karaman, Turkey, [f]Chemical Engineering Department, Middle East Technical University, 06531 Ankara, Turkey, and [g]Food Engineering Department, Middle East Technical University, 06531 Ankara, Turkey

Correspondence e-mail: m.j.mcpherson@leeds.ac.uk

Received 24 October 2012
Accepted 29 November 2012

PDB References: CATPO, native, 4aue; recombinant, 4aum; H82N variant, 4aul; V123F variant, 4aun

Scytalidium thermophilum produces a catalase with phenol oxidase activity (CATPO) that catalyses the decomposition of hydrogen peroxide into oxygen and water and also oxidizes various phenolic compounds. A codon-optimized *catpo* gene was cloned and expressed in *Escherichia coli*. The crystal structures of native and recombinant *S. thermophilum* CATPO and two variants, H82N and V123F, were determined at resolutions of 2.7, 1.4, 1.5 and 1.9 Å, respectively. The structure of CATPO reveals a homotetramer with 698 residues per subunit and with strong structural similarity to *Penicillium vitale* catalase. The haem component is *cis*-hydroxychlorin γ-spirolactone, which is rotated 180° with respect to small-subunit catalases. The haem-binding pocket contains two highly conserved water molecules on the distal side. The H82N mutation resulted in conversion of the native *d*-type haem to a *b*-type haem. Kinetic studies of the H82N and V123F mutants indicate that both activities are likely to be associated with the haem centre and suggest that the secondary oxidase activity may be a general feature of catalases in the absence of hydrogen peroxide.

1. Introduction

Catalases (hydrogen peroxide:hydrogen peroxide oxidoreductases; EC 1.11.1.6) are haem-containing enzymes that are present in most aerobic organisms (Goldberg & Hochman, 1989; Nicholls *et al.*, 2001). They serve to protect cells against reactive oxygen species by degrading hydrogen peroxide to water and oxygen (1) (Switala & Loewen, 2002; Chelikani *et al.*, 2004; Maté *et al.*, 2001; Nicholls *et al.*, 2001),

$$2H_2O_2 \rightarrow 2H_2O + O_2. \quad (1)$$

This catalytic reaction occurs in two distinct stages (Chelikani *et al.*, 2004). The first stage involves the oxidation of the haem by the first hydrogen peroxide to form an oxyferryl species and a porphyrin cation radical (2). In the second stage, this radical intermediate, known as compound I, is reduced by a second hydrogen peroxide to regenerate the resting-state enzyme, water and oxygen (3) (Switala & Loewen, 2002; Nicholls *et al.*, 2001),

$$\text{Enz (Por}-\text{Fe}^{\text{III}}) + H_2O_2 \rightarrow \text{compound I (Por}^{+\bullet}-\text{Fe}^{\text{IV}}{=}\text{O}) + H_2O, \quad (2)$$

$$\text{Compound I (Por}^{+\bullet}-\text{Fe}^{\text{IV}}{=}\text{O}) + H_2O_2 \rightarrow \text{Enz (Por}-\text{Fe}^{\text{III}}) + H_2O + O_2. \quad (3)$$

At limiting H_2O_2 concentrations and in the presence of a suitable organic donor, catalases may function as peroxidases

by catalyzing the one-electron reduction of compound I to form compound II (4),

$$\text{Compound I (Por}^{+\bullet}\text{–Fe}^{\text{IV}}\text{=O)} + AH_2 \rightarrow \text{compound II (Por–Fe}^{\text{IV}}\text{–OH)} + A\text{H}^{\bullet}, \quad (4)$$

$$\text{Compound II (Por–Fe}^{\text{IV}}\text{–OH)} + AH_2 \rightarrow \text{Enz (Por–Fe}^{\text{III}}\text{)} + A\text{H}^{\bullet}.$$

The catalase reaction has evolved in four phylogenetically unrelated enzyme classes: the monofunctional or typical catalases, the bifunctional catalase–peroxidases, the nonhaem manganese-containing catalases and the minor catalases (Maté *et al.*, 2001; Nicholls *et al.*, 2001). The largest and most extensively studied group are the monofunctional catalases, which can be subdivided into those with large (75–84 kDa) subunits containing haem *d* and those with small (55–69 kDa) subunits containing haem *b*. The crystal structures of 14 monofunctional haem-containing catalases from different sources have been reported, including bovine liver (Fita *et al.*, 1986; Murthy *et al.*, 1981), *Enterococcus faecalis* (Håkansson *et al.*, 2004), *Escherichia coli* (Bravo *et al.*, 1995, 1999), *Exiguobacterium oxidotolerans* (Hara *et al.*, 2007; Díaz *et al.*, 2012), *Helicobacter pylori* (Loewen *et al.*, 2004), human erythrocytes (Ko *et al.*, 2000; Putnam *et al.*, 2000), *Micrococcus lysodeikticus* (Murshudov *et al.*, 1992), *Neurospora crassa* (Díaz *et al.*, 2004), *Penicillium vitale* (Vainshtein *et al.*, 1981, 1986), *Pichia angusta* (Peña-Soler *et al.*, 2011; Díaz *et al.*, 2011), *Proteus mirabilis* (Gouet *et al.*, 1995), *Pseudomonas syringae* (Carpena *et al.*, 2003), *Saccharomyces cerevisae* (Maté *et al.*, 1999) and *Vibrio salmonicida* (Riise *et al.*, 2007; Díaz *et al.*, 2012). The haem-containing catalases are generally homotetramers with molecular masses ranging from ∼220 to ∼330 kDa (Chelikani *et al.*, 2004; Nicholls *et al.*, 2001; Klotz & Loewen, 2003). They exhibit strong absorbance in the Soret band (406 nm) and have an Rz (A_{406}/A_{280}) value of around 1 (Zámocký & Koller, 1999). The haem prosthetic groups are either a noncovalently bound iron protoporphyrin IX (haem *b*) or an oxidized form of protoporphyrin IX (haem *d*) (Maté *et al.*, 2001). Haem *d* contains a *cis*-hydroxy γ-spirolactone that is rotated 180° about the axis defined by the α–γ *meso*-C atoms when compared with the orientation found for haem *b* in bovine liver catalase (Fig. 1; Murshudov *et al.*, 1996). Although the origin of haem *d* has not been determined, it has been suggested that the enzyme is likely to first bind haem *b*, which is subsequently converted to haem *d* through oxidation by the first H_2O_2 molecules bound to the enzyme (Timkovich & Bondoc, 1990). In hydroperoxidase II this has been shown to be catalyzed by the enzyme itself in the presence of hydrogen peroxide (Maté *et al.*, 2001; Timkovich & Bondoc, 1990; Loewen *et al.*, 1993; Bravo *et al.*, 1997) or singlet oxygen (Díaz *et al.*, 2005) with the requirement of a distal histidine (Loewen *et al.*, 1993).

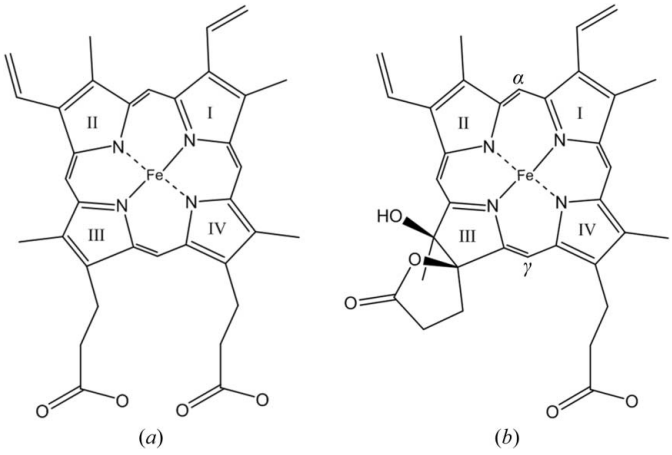

Figure 1
Structures of (*a*) haem *b* and (*b*) haem *d*.

At low concentrations of hydrogen peroxide some catalases have been shown to possess additional peroxidase activity, demonstrating the ability to oxidize low-molecular-weight alcohols (Nicholls *et al.*, 2001). In the absence of hydrogen peroxide, a further oxidative activity has been documented by Vetrano *et al.* (2005) for a mammalian catalase. The authors showed that the enzyme oxidized several functionally important phenolic compounds, suggesting a significant biological role for this dual activity (Vetrano *et al.*, 2005). A second example of such a dual-function catalase–oxidase is the bifunctional catalase–phenol oxidase (CATPO) that has been characterized from the thermophilic fungus *Scytalidium thermophilum* (Sutay Kocabas *et al.*, 2008). In addition to its major function as a catalase, CATPO also has minor oxidizing activity towards various phenolic compounds in the absence of hydrogen peroxide (Sutay Kocabas *et al.*, 2008; Ögel *et al.*, 2006).

S. thermophilum CATPO is a homotetramer with a molecular mass of 320 kDa. We have previously reported the crystallization of this enzyme (Sutay Kocabas *et al.*, 2009). Here, we report the crystallographic structure determination of this enzyme at 2.7 Å resolution.

Several residues in the haem pocket are highly conserved amongst haem-containing catalases, including an essential histidine and valine situated on the distal side of the haem. The histidine is essential for catalysis, acting as an acid–base catalytic group (Loewen *et al.*, 1993), whilst the valine is responsible for narrowing the channel that connects the active site to the exterior of the enzyme (Maté *et al.*, 1999). With the aim of understanding the basis for the phenol oxidase activity of CATPO, we have expressed a codon-optimized *catpo* gene from *S. thermophilum* in *E. coli* and have studied two mutant forms of CATPO: H82N and V123F (the essential histidine and valine). The structures of the recombinant wild type (*r*CATPO) and of the two mutants have been determined at 1.4, 1.5 and 1.9 Å resolution, respectively.

2. Experimental procedures

2.1. Expression and purification of native CATPO

Cultures of *S. thermophilum* (type culture *Humicola insolens*, ATCC No. 16454) were grown in modified YpSs growth medium containing 4 g l^{-1} yeast extract, 1 g l^{-1} K_2HPO_4,

0.5 g l^{-1} $MgSO_4 \cdot 7H_2O$, 0.1 g l^{-1} $CuSO_4 \cdot 5H_2O$ and 40 g l^{-1} glucose. *S. thermophilum* was grown for 5 d at 318 K with shaking at 155 rev min^{-1}. Cells were removed by centrifugation at 10 000 rev min^{-1} for 10 min (277 K) and the supernatant containing CATPO was precipitated with 60%(*w*/*v*) ammonium sulfate and dialyzed against 50 m*M* Tris–HCl pH 8.0 overnight at 277 K. The dialyzed suspension was filtered (0.2 µm) to remove any precipitate before further purification.

S. thermophilum CATPO was purified to homogeneity by adopting a two-step procedure including anion-exchange and gel-filtration chromatography using an ÄKTAprime FPLC system (Amersham Pharmacia) at 277 K. Ion exchange was performed by packing Q Sepharose High Performance medium (GE Healthcare, USA) into an XK 16/20 column (GE Healthcare) followed by equilibration with 50 m*M* Tris–HCl pH 8.0 at a flow rate of 1 ml min^{-1}. The column was washed several times with the same buffer and CATPO was eluted with a linear gradient of 0–0.4 *M* NaCl in 50 m*M* Tris–HCl pH 8.0. The presence and purity of CATPO were confirmed by SDS–PAGE and the combined eluates were dialyzed against 50 m*M* Tris–HCl pH 8.0 alone to remove salt and concentrated using a 10K centrifugal concentrator (Microsep, USA) prior to gel filtration. Gel filtration was carried out using a HiPrep 26/60 Sephacryl S-200 high-resolution column (GE Healthcare, USA) in 50 m*M* Tris–HCl pH 8.0 at a flow rate of 1 ml min^{-1}. CATPO-containing fractions were pooled and concentrated as before.

2.2. *E. coli* strains, media and cultivation

E. coli XL-1 Blue (Stratagene) and BL21 Star (DE3) (Invitrogen) strains were used for cloning and expression, respectively. During cloning steps, *E. coli* cells were grown aerobically at 310 K in LB medium supplemented with 50 µg ml^{-1} kanamycin.

2.3. Molecular cloning

Based on the exon nucleotide sequence of the *S. thermophilum* catalase gene (Moyer, 1997), an *E. coli* codon-optimized sequence of the *catpo* gene-coding region was synthesized and cloned into pUC57 (GenScript Corporation, USA) for recombinant expression in *E. coli*. A forward primer (5′-GGAATTC**CATATG**ACCTGCCCGTTCGCTGACCCG-3′; the 5′-*Nde*I site is shown in bold) and a reverse primer (5′-C**AAGCTT**GGGTTAAGAGTCCAGAGCGAAACG-GTC-3′; the 3′-*Hin*dIII site is shown in bold) were designed to PCR-amplify the *catpo* gene from pUC57 excluding the first 19 codons encoding the N-terminal signal peptide. The cleavage site of the signal peptide was predicted using the *SignalP* 3.0 server (Bendtsen *et al.*, 2004; Nielsen *et al.*, 1997). The region coding for the mature *catpo* gene was PCR-amplified using KOD DNA polymerase (Novagen) under the following conditions: initial denaturing at 368 K for 2 min followed by 30 cycles of 368 K for 1 min, 333 K for 1 min and 345 K for 2.5 min and a final 10 min extension phase at 345 K. The PCR product was gel-purified (QIAquick gel extraction kit, Qiagen), double restriction-digested with *Nde*I and *Hin*dIII (NEB), subcloned into pET28aTEV (kindly provided by Dr John Taylor and Professor R. E. Sockett, University of Nottingham) and transformed into competent *E. coli* XL-1 Blue cells. Positive clones were confirmed by restriction analysis and DNA sequencing. The construct, which carried an N-terminal 6×His tag sequence and a TEV protease cleavage site, was designated pET28a-CATPO.

2.4. Site-directed mutagenesis

Single-point mutations were introduced into the *catpo* coding region by QuikChange (Stratagene) using mutagenic primer pairs, substituting *Pfu* DNA polymerase for KOD DNA polymerase (Novagen), for 30 cycles prior to *Dpn*I digestion. Primers containing the desired single mutations were as follows (sense only): 5′-CGGAACGTGCTGT-TAACGCTCGTGGTGC (H82N) and 5′-CGTTCGTTTCT-CTACCTTCGCTGGTTCTCGTGGTTCTGC (V123F).

The introduction of the H82N and V123F mutations was confirmed by DNA sequencing.

2.5. Protein overexpression and purification

pET28a-CATPO was freshly transformed into *E. coli* BL21 Star (DE3) cells and a single colony was inoculated into 10 ml LB medium supplemented with 50 µg ml^{-1} kanamycin and incubated overnight at 310 K with shaking (200 rev min^{-1}). The entire overnight culture was used to inoculate 1 l LB medium supplemented with 50 µg ml^{-1} kanamycin in a 2.4 l conical flask and was grown at 310 K (200 rev min^{-1}) until an OD_{600} of 0.6–0.8 was reached, at which point IPTG (0.1 m*M* final concentration) was added and incubation was continued at 303 K (120 rev min^{-1}) for 24 h to achieve semi-anaerobic conditions. The cells were then harvested by centrifugation for 10 min at 6000 rev min^{-1} (277 K) and the pellets were frozen at 193 K until use. Following thawing of the pellet, the cells were lysed using 100 ml lysis buffer [50 m*M* Na HEPES, 25%(*w*/*v*) sucrose, 1%(*v*/*v*) Triton X-100, 5 m*M* $MgCl_2 \cdot 6H_2O$] per litre of original culture. The suspension was centrifuged at 10 000 rev min^{-1} for 30 min (277 K) and the supernatant was either used as a crude enzyme solution for activity assays or dialyzed overnight against 20 m*M* sodium phosphate buffer pH 7.4, 0.5 *M* NaCl. The dialyzed fraction was filtered (0.2 µm) and loaded onto a HiTrap Chelating HP column (1 ml; GE Healthcare) pre-charged with Ni^{2+} and pre-equilibrated with 20 m*M* sodium phosphate, 0.5 *M* NaCl, 20 m*M* imidazole pH 7.4 using a Gradifrac Purifier (GE Healthcare, USA). Recombinant 6×His-CATPO was purified by affinity chromatography by applying a wash step (20 m*M* sodium phosphate, 0.5 *M* NaCl, 100 m*M* imidazole pH 7.4) followed by elution, collecting 1 ml fractions over a 50 ml linear gradient from 0.1 to 0.5 *M* imidazole. Each fraction was tested for purity by SDS–PAGE and the concentration of the pooled fractions was determined by the Bradford assay using bovine serum albumin as a standard.

Table 1
Crystallographic data-collection and refinement statistics.

Values in parentheses are for the outermost shell.

	S. thermophilum CATPO	*r*CATPO	H82N variant	V123F variant
PDB code	4aue	4aum	4aul	4aun
Diamond beamline	I03	I04-1	I02	I04
Wavelength (Å)	0.97	0.92	0.98	0.95
Space group	$P2_12_12$	$C2$	$C2$	$C2$
Unit-cell parameters				
a (Å)	185.4	201.4	201	253.3
b (Å)	216.3	121.4	121.9	243.4
c (Å)	68.6	125.2	124.9	97.1
Resolution (Å)	141.4–2.70 (2.77–2.70)	113.0–1.40 (1.44–1.40)	28.96–1.50 (1.54–1.50)	69.94–1.90 (1.97–1.90)
$R_{\rm merge}$† (%)	9.8 (45.0)	7.2 (43.4)	5.9 (44.4)	12.6 (53.9)
$R_{\rm p.i.m.}$‡ (%)	4.1 (19.0)	2.9 (17.3)	5.4 (40.5)	8.2 (34.7)
Observed reflections	50325	3598880	787895	1485328
Unique reflections	76826	506416	417266	444158
Completeness (%)	99.9 (100)	95.3 (94.7)	96.4 (97.2)	99.8 (100.0)
Multiplicity	6.5 (6.6)	7.1 (7.1)	1.9 (1.8)	3.3 (3.3)
$\langle I/\sigma(I)\rangle$	13.3 (4.0)	16.2 (4.4)	6.0 (1.8)	7.6 (2.4)
Refinement				
R factor (%)	19.2 (28.5)	11.8 (17.1)	14.3 (25.0)	16.4 (24.6)
$R_{\rm free}$§ (%)	25.1 (34.9)	14.5 (21.2)	19.3 (32.1)	20.0 (29.1)
No. of protein atoms	21017	22242	21715	42801
No. of solvent molecules	316	2463	2497	3405
No. of ligand atoms	471	176	172	361
Average overall B factor (Å^2)	49.0	13.2	13.6	15.3
R.m.s.d., bond lengths¶ (Å)	0.011	0.010	0.016	0.006
R.m.s.d., bond angles¶ (°)	1.6	1.5	1.9	1.1
Ramachandran analysis, residues in regions of the plot (%) ††				
Most favoured	95	97	96	96
Outliers	0.3	0.5	0.6	0.5

† $R_{\rm merge} = \sum_{hkl}\sum_i |I_i(hkl) - \langle I(hkl)\rangle| / \sum_{hkl}\sum_i I_i(hkl)$. ‡ $R_{\rm p.i.m.}$ is the precision-indicating (multiplicity-weighted) $R_{\rm merge}$ relative to $I+$ or $I-$. § $R_{\rm free}$ was calculated with 5% of reflections set aside randomly. ¶ Based on the ideal geometry values of Engh & Huber (1991). †† Ramachandran analysis using the program *MolProbity* (Chen *et al.*, 2010).

2.6. Enzyme-activity assay

Catalase and phenol oxidase activity assays were performed using a temperature-controlled spectrophotometer (Shimadzu UV-2401). All assays were performed in triplicate in 100 m*M* sodium phosphate buffer pH 7.0 at 333 K. Specific activity assays for catalase activity were carried out using 10 m*M* H_2O_2 as a substrate and enzyme activity was determined using the initial rate of the reaction, monitoring the decrease in absorbance at 240 nm [$\varepsilon_{240}(H_2O_2)$ of 39.4 M^{-1} cm^{-1}; Merle *et al.*, 2007]. One unit of activity was defined as the amount of enzyme that catalysed the decomposition of 1 µmol H_2O_2 per minute. Phenol oxidase activity was determined by monitoring the increase in absorbance at 420 nm using 100 m*M* catechol as a substrate. Enzyme activity was determined using the initial rate of the reaction and an extinction coefficient at 420 nm of 3450 M^{-1} cm^{-1} for catechol (Ögel *et al.*, 2006), where one unit of activity corresponds to the formation of one nanomole of product per minute.

2.7. UV–Vis spectra

All spectroscopic measurements were performed using a Shimadzu 2401PC UV–Vis spectrophotometer at room temperature. Absorption spectra of purified native, recombinant wild type and mutational variants were recorded in a quartz cuvette (1 cm path length) at between 200 and 900 nm.

2.8. Comparison of *r*CATPO catalase and phenol oxidase activities with those of catalases from different sources

In addition to purified *S. thermophilum r*CATPO, catalases from four different sources (*A. niger*, human erythrocytes, *Corynebacterium glutamicum* and bovine liver) were obtained from Sigma–Aldrich, Germany and assayed for catalase and phenol oxidase activity.

2.9. Crystallization, data collection and refinement

Crystals of native CATPO that were improved in size and diffraction capability with respect to those reported previously (Sutay Kocabas *et al.*, 2009) were obtained at 291 K by the sitting-drop vapour-diffusion method using a protein concentration of 9.4 mg ml^{-1} and a reservoir solution consisting of 18%(*w*/*v*) PEG 2000, 0.1 *M* barium chloride, 0.1 *M* bis-tris pH 6.8. Prior to flash-cooling the crystal in liquid nitrogen for diffraction analysis, 45%(*w*/*v*) PEG 2000 (final concentration) was added to the mother-liquor droplet containing the brownish-green crystals and was left overnight to diffuse. Diffraction data were collected using synchrotron radiation of wavelength 0.97 Å on beamline I03 at Diamond Light Source, England (Table 1). The diffraction data were processed using *MOSFLM* (Leslie, 1999), scaled with *SCALA* (Evans, 1997, 2011) and reduced using *SCALA* and *TRUNCATE* from the *CCP*4 program suite (Winn *et al.*, 2011). Structure determination of native CATPO was carried out with the program *MOLREP* (Vagin & Teplyakov, 2010) using the native *P. vitale*

catalase (PVC) structure as the search model (PDB entry 2iuf; Alfonso-Prieto *et al.*, 2007). Model building and refinement were performed using *Coot* (Emsley *et al.*, 2010) and *REFMAC*5 (Murshudov *et al.*, 2011) with the application of fourfold NCS.

Diamond-shaped crystals of recombinant wild-type CATPO (*r*CATPO) and the H82N variant were obtained by vapour diffusion against reservoirs consisting of 6–16%(*w*/*v*) PEG 400, 0.2 *M* potassium chloride, 0.01 *M* calcium chloride, 0.05 *M* sodium cacodylate pH 5.0–5.6. Crystals of the V123F variant were obtained under similar conditions except that PEG 4000 was used as a precipitant rather than PEG 400. Good-quality crystals were then flash-cooled in liquid nitrogen after soaking in 20%(*v*/*v*) PEG 400 (final concentration). The diffraction data were also collected at Diamond Light Source at 100 K (beamlines I02, I04-1 and I04), followed by autoindexing and integration using *XDS* (Kabsch, 2010). Subsequent steps were carried out using the *CCP*4 suite (Winn *et al.*, 2011). The crystal structure of V123F was determined using the native structure of CATPO as a molecular-replacement model. The crystal structure of *r*CATPO was then determined using the V123F structure as a molecular-replacement model, and this was then used to phase the H82N variant data.

All figures were prepared using *PyMOL* (http://pymol.org/). The structure factors and coordinates have been submitted to the Protein Data Bank with accession codes 4aue for native CATPO, 4aum for *r*CATPO, 4aul for the H82N variant and 4aun for the V123F variant.

3. Results

3.1. Characterization of CATPO variants

Recombinant wild-type and mutational variants of CATPO appeared as single bands at an apparent molecular weight of 79 kDa as determined by SDS–PAGE (Fig. 2). Both purified native and recombinant CATPO were green in colour, indicative of a *d*-type haem prosthetic group. The UV–Vis spectrum of native CATPO had absorption maxima at 280, 402, 592 and 691 nm (Fig. 2), with an Rz value (A_{402}/A_{280}) of ∼0.5, which is consistent with the haem content reported previously for native CATPO (Sutay Kocabas *et al.*, 2008). The phenol oxidase activities of native and recombinant CATPO were approximately the same, except that the recombinant wild-type enzyme exhibited a twofold higher catalase activity. UV–Vis spectroscopy of the recombinant wild-type CATPO also showed four major peaks at 280, 406, 590 and 714 nm; consistent with its increased catalase activity, the recombinant enzyme had an increased Rz value of 0.9.

To investigate the basis of the dual functionality of CATPO with phenol oxidation and catalase activities, whether both catalytic reactions occur at the prosthetic haem centre and whether catalysis requires a *d*-type haem, we generated mutational variants designed to target two conserved residues, His82 and Val123, both of which are conserved in almost all monofunctional catalases (Murshudov *et al.*, 1996). Two variants were generated: H82N and V123F. His82 lies dorsal to the haem *d* and is absolutely required for activity (Melik-Adamyan *et al.*, 2001). Mutation of this residue to asparagine in *E. coli* HPII catalase has been shown to result in a *b*-type protohaem bound in place of the haem *d* (Obinger *et al.*, 1997). The residue equivalent to Val123 in the HPII catalase (Val169) lies in the channel above His82 and mutation of this residue in HPII has been shown to result in a 12-fold reduction in catalase activity whilst retaining haem *d* (Chelikani *et al.*, 2003).

Table 2
Specific activities of purified CATPO variants.

Variant	Specific activity	
	Catalase (μmol mg^{-1} min^{-1})	Phenol oxidase (nmol mg^{-1} min^{-1})
S. thermophilum CATPO	8870 ± 1000	194 ± 5
*r*CATPO	18713 ± 935	213 ± 5
H82N	4 ± 0.6	50 ± 13
V123F	65 ± 6	22 ± 1

Purified H82N CATPO was red in colour, with an Rz value of 0.8 that was consistent with that of *r*CATPO, indicating substantial haem content. H82N CATPO demonstrated extremely low catalase and reduced phenol oxidase activities

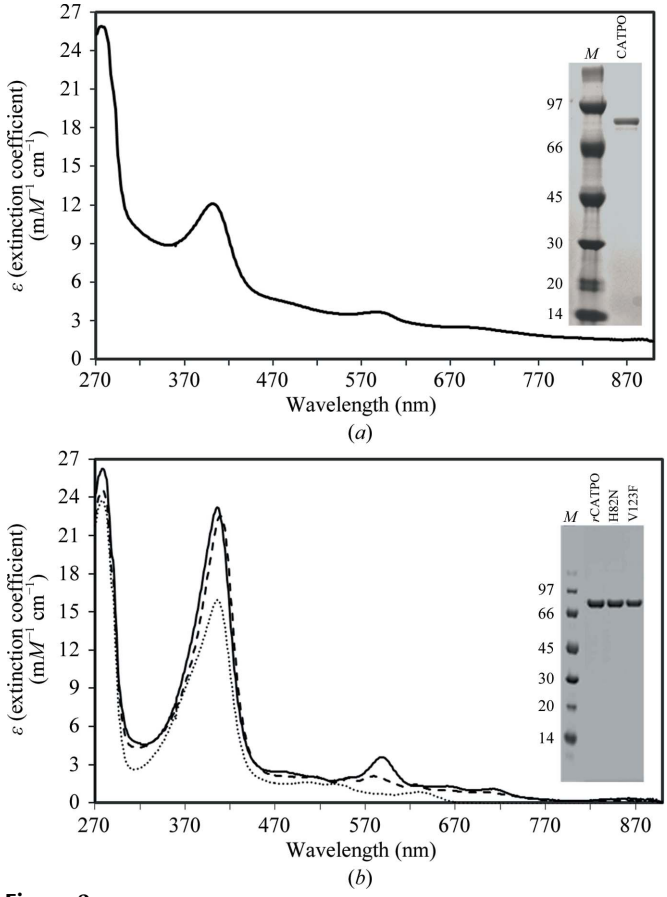

Figure 2
(*a*) UV–Vis spectrum of native CATPO from *S. thermophilum*. (*b*) Comparison of the UV–Vis spectra of *r*CATPO and the H82N and V123F variants. Insets, Coomassie-stained SDS–PAGE gels showing the purity of the CATPO variants. Lanes *M* contain molecular-mass markers (labelled in kDa).

of 0.02% and 23% of those of *r*CATPO (Table 2). Consistent with its red colour, H82N had λ_{max} values at 280, 406, 536 and 629 nm; the absence of the characteristic haem *d* peak at 590 nm indicates a lack of haem *d* and the presence of (proto)haem *b*. In contrast, purified V123F CATPO was green in colour and had an identical Rz value to the H82N variant, yet it displayed identical spectral features to *r*CATPO, with λ_{max} values at 280, 406, 590 and 714 nm, indicating the presence of haem *d*. However, both catalytic activities of the V123F variant were substantially reduced to 0.3% of the catalase activity and 10% of the phenol oxidase activity relative to *r*CATPO (Table 2).

Table 3
Comparison of CATPO catalase (CAT) and phenol oxidase (PO) activities with those of other catalases.

Catalase source	CAT activity (µmol mg^{-1} min^{-1})	PO activity (nmol mg^{-1} min^{-1})
*r*CATPO	18713 ± 935	213 ± 5
A. niger	3502 ± 321	20 ± 0.4
C. glutamicum	53315 ± 692	204 ± 4
Bovine liver	6125 ± 1027	73 ± 1.6
Human erythrocytes	98477 ± 4652	1342 ± 25

3.2. Comparison of the oxidase activities of catalases from different sources

To examine whether catalase/phenol oxidase dual activity is a more general property of catalases, commercially available catalases from *A. niger*, human erythrocytes, *C. glutamicum* and bovine liver were purchased. Human erythrocyte catalase showed the highest enzymatic activity, with the *C. glutamicum* catalase being the second most active and the *S. thermophilum* catalase the third, whilst the *A. niger* and bovine liver catalases showed the lowest activities (Table 3).

Surprisingly, all four commercial enzymes showed phenol oxidase activity when assayed with catechol (Table 3). The phenol oxidase efficiencies of the human, bovine liver and *S. thermophilum* catalases were found to be approximately 1.4, 1.2 and 1.14% with respect to their catalase activities, whilst the *A. niger* catalase demonstrated an ∼50% lower phenol

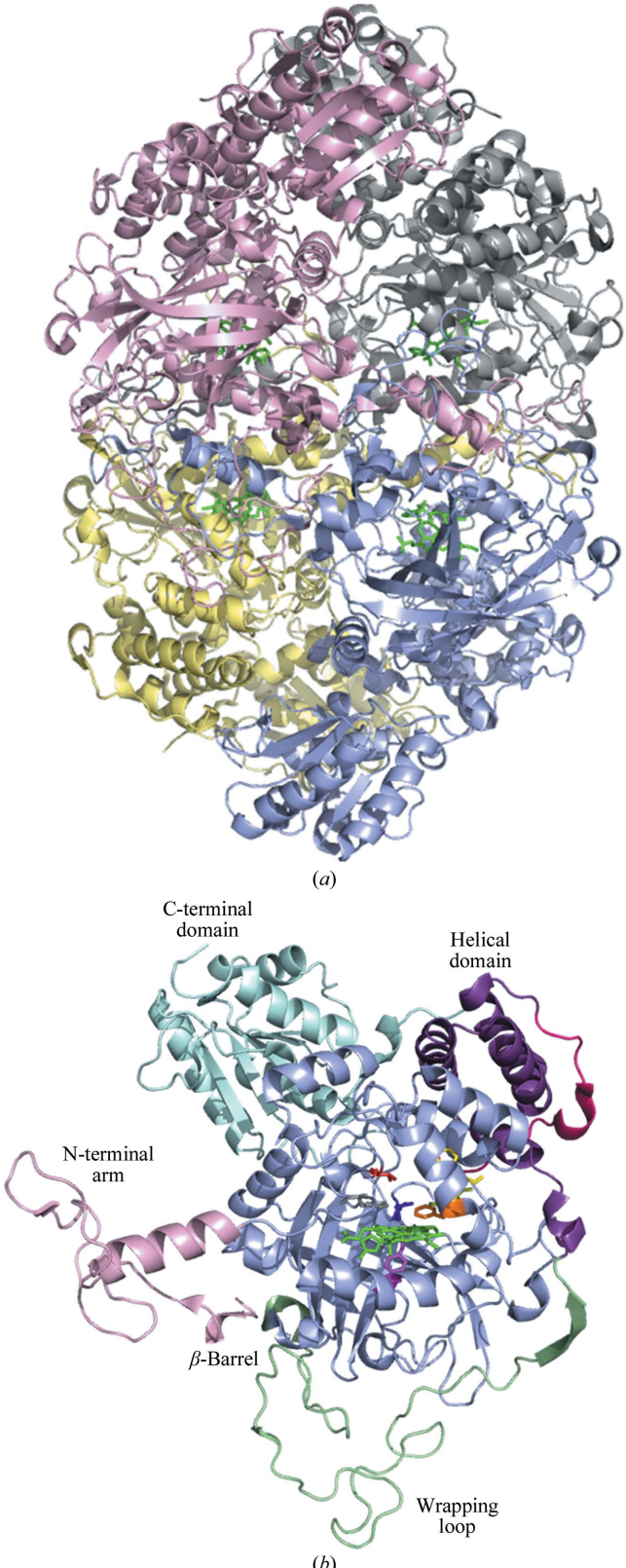

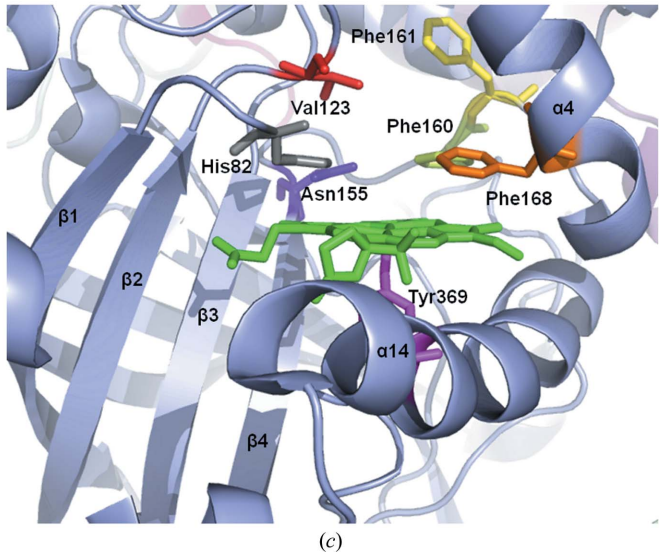

Figure 3
Structure of the *r*CATPO tetramer (*a*), monomer (*b*) and active centre (*c*). The haem is coloured green, Tyr369 magenta, His82 grey, Asn155 purple/blue, Val123 red, Phe160 lemon, Phe161 yellow and Phe168 orange.

oxidation efficiency than that of *S. thermophilum* at ∼0.6%. The least phenol oxidase active catalase tested was that from *C. glutamicum*, at 0.4%.

3.3. Quality of the structural models

The electron-density map of the native enzyme defines the main-chain and side-chain atoms of 2679 amino acids, 316 water molecules and 21 di-*N*-acetylglucosamine (NAG) moieties. The map shows clear continuity in all subunits over the backbone chain from Glu27 to Asp697. The 26 residues at the N-terminus predicted from the gene sequence are disordered in all four subunits. Ser698 in subunits *A* and *C* was not modelled owing to weak density. The following regions are disordered: Ala618–Ala621 in subunits *A* and *C*, Ala618–Thr620 in subunit *B* and Ala618–Ser622 in subunit *D*. The final model was refined at 2.7 Å resolution with fourfold NCS restraints.

The *r*CATPO structure contains four subunits with 2694 amino acids, four haem groups and 2463 water molecules. The map shows continuity in almost all subunits over the complete length from Ser21 to Asp697. Ser698 in all subunits except *B* was not modelled owing to weak density. The following loops are disordered: Phe617–Ser622 in subunits *A* and *B* and Ala618–Ser622 in subunits *C* and *D*. Apart from the lack of glycosylation, the native and recombinant wild-type CATPO structures have an r.m.s.d. over all atoms of 0.35 Å and are essentially the same. Similar to the structure of *r*CATPO, the mutants analysed here, H82N and V123F, are also homotetramers with 2690 amino acids. In addition to similar disordered regions to *r*CATPO, the loop between residues Gly650 and Val655 could not be modelled owing to weak density. The N-terminal 20 residues of all subunits in all three structures (*r*CATPO, H82N and V123F) were disordered as in the wild-type native enzyme and were not included in the final refined models. Data and model quality statistics are summarized in Table 1.

The quality and resolution of the diffraction data are considerably better for *r*CATPO than for the native protein; therefore, the structure of the recombinant protein will be further discussed here.

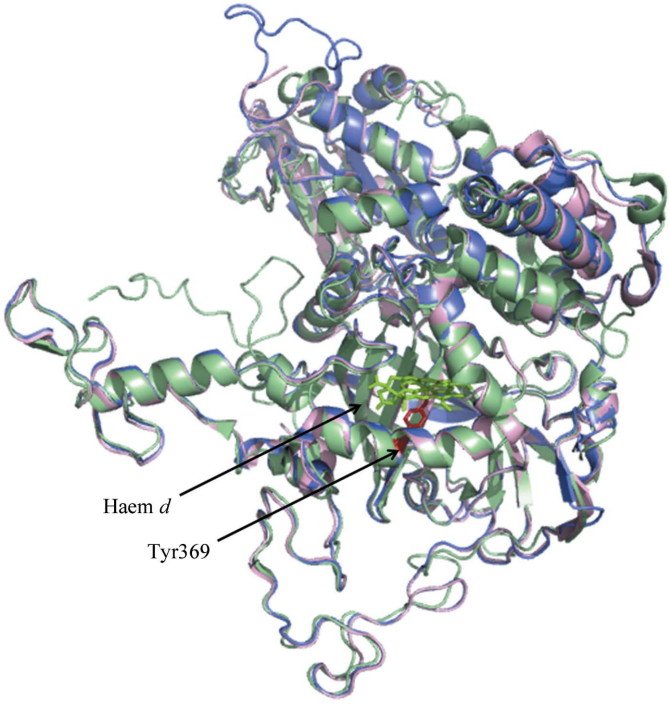

Figure 4
Comparison of the *S. thermophilum* CATPO, *P. vitale* catalase (PVC) and HPII structures. View of chain *A* of HPII (PDB entry 1gge; Melik-Adamyan *et al.*, 2001) and PVC (PDB entry 2iuf; Alfonso-Prieto *et al.*, 2007) superposed onto *r*CATPO (PDB entry 4aum; this work). Light pink, *S. thermophilum* CATPO; blue, PVC; pale green, HPII; green, haem centre; red, Tyr369.

3.4. Overall structure

*r*CATPO crystallizes with a homotetramer in the asymmetric unit in space group *C*2, with unit-cell parameters a = 201.4, b = 121.4, c = 125.2 Å. The *r*CATPO monomer is similar to those described for other catalases (Bravo *et al.*, 1999; Vainshtein *et al.*, 1986; Díaz *et al.*, 2009) and is composed of five different regions: a long amino-terminal arm, an antiparallel eight-stranded β-barrel, an extended wrapping loop, a four-helical domain and, as in large catalases, a carboxy-terminal domain with flavodoxin-like topology joined by a long loop (Fig. 3).

*r*CATPO was purified using an N-terminal His tag; however, Ser21 is the first residue that is visible in the crystal structure, suggesting that the 20 N-terminal residues and the His tag are disordered. The amino-terminal domain (Ser21–Glu74) is entirely buried by neighbouring subunits. The haem-binding domain is a β-barrel consisting of eight antiparallel β-strands accompanied by several helical segments of one to four turns each. The first half of the β-barrel (residues Gly138–Asn155) is involved in forming the substrate-access channel cavity on the distal side of the haem. The extended wrapping loop of 64 residues (Pro386–Arg449) connects the β-barrel and α-helical regions. This region lacks secondary structure in a long stretch of polypeptide chain between residues 389 and 442, whilst the remainder is mostly comprised of α-helices. Fungal catalases have six or seven prolines in the wrapping loop, which are represented in CATPO by Pro386, *cis*-Pro416 and *cis*-Pro424, which are also structurally conserved in PVC (*P. vitale*), HPII (*E. coli*) and CAT-3 (*N. crassa*). Three other prolines, Pro390, Pro393 and Pro439, are also conserved in PVC, whereas only one, Pro413, is present in CATPO, in which this domain ends with one β-strand close to the α-helical domain.

The α-helical domain contains 70 residues (Glu450–Gly519) forming four antiparallel contiguous helices (α18–α21), where α18 and α20 form the site for NADPH binding in small-subunit catalases such as BLC. However, in large-subunit catalases such as CATPO the hydrophilic environment of the coil responsible for connecting to the carboxy-terminal region prevents NADPH binding (Díaz *et al.*, 2004).

The carboxy-terminal domain contains 179 amino-acid residues (Ala520–Ser698) and is highly structured with an α/β

arrangement with mainly parallel β-strands in a 'flavodoxin-like' topology.

3.5. Comparison of CATPO with HPII and PVC

Main-chain structural alignment of CATPO, HPII and PVC reveals extensive structural conservation (Fig. 4*a*). The β-barrel, wrapping loop and α-helical domain are almost identical in CATPO, HPII and PVC. The major differences between these enzymes are located in the N-terminal and C-terminal regions. HPII has a longer amino-terminal arm than both CATPO and PVC (Fig. 4). The extended nature of the amino-terminal region in HPII has been proposed to be responsible for its enhanced stability at high pH and high temperature (Sevinc *et al.*, 1995). This might be a consequence of the additional presence of three helices and two β-sheets in HPII, whereas CATPO has only one α-helix and no β-sheets.

The carboxy-terminal domain of large catalases has low sequence similarity but has a conserved general structure (Supplementary Fig. 1[1]). PVC and HPII have nine more amino-acid residues than CATPO and the C-terminal end has a different orientation in HPII than in CATPO and PVC.

3.6. Haem pocket

The four haem molecules are deeply buried inside the CATPO tetramer at about 22 Å from the nearest solvent-exposed surface, as in other haem-containing catalases for which structures have been determined (Maté *et al.*, 2001; Bravo *et al.*, 1997). The haem lies between the β-barrel (β1–β4) and helices α4 and α14 (Fig. 3). In CATPO, as in other catalases, the propionic acids of the haem make salt bridges to three conserved arginine residues (Arg79 and Arg119 in β2 and Arg365 in α14).

As in PVC and HPII, the haem *d* group identified in the active centre of CATPO has a *cis*-hydroxy γ-spirolactone structure which can be clearly observed in the electron-density map. The presence of the γ-spirolactone ring and hydroxyl group make the haem *d* more asymmetric with respect to the haem *b* found in small clade 3 catalases.

On the proximal side of the haem, Tyr369 forms the fifth coordination bond to the iron. There does not appear to be a direct coordination of water to the iron in the sixth coordination position because the closest water molecule is 2.3 Å away in all subunits. This is consistent with the spectral data reported here and for other haem *d* catalases, which indicate that these enzymes contain a five-coordinate high-spin ferric iron (Loewen *et al.*, 2004). The tyrosine phenolate also makes a hydrogen bond to Arg365 (Fig. 5). On the distal side, the imidazole ring of His82 lies almost parallel to the haem above pyrrole ring IV. The N^{δ} atom of His82 forms a hydrogen bond to the Ser121 hydroxyl. The N^{ε} atom of this essential histidine also forms a hydrogen bond to a water molecule (W2). As observed in other large catalases, His82 is stabilized by Arg119 and Val123 through hydrogen bonds to its main-chain O atom and N atom, respectively (Fig. 5).

The water molecules W1 and W2 are bound to either the haem or amino-acid residues of the haem pocket. W1 interacts with the two haem propionic acid groups, while W2 interacts with the N^{ε} atom of His82 and water molecules W1 and W3. Three other water molecules (W9–W11) are located in the channel leading away from the haem pocket towards the protein surface. Two are close to the amino-terminal arm and one is in the carboxy-terminal region (Fig. 5).

3.7. Structural differences of the CATPO variants with respect to the wild-type enzyme

The three-dimensional structures of the H82N and V123F variants of CATPO were determined and refined at 1.5 and 1.9 Å resolution, respectively. In contrast to the native CATPO, *r*CATPO and H82N crystal forms, the V123F crystals contain one tetramer and two dimers in each asymmetric unit. The dimers are parts of tetramers that lie on the crystallographic twofold axis. The final refined structures provided a clear electron-density map that revealed significant differences in both the variant residue and the haem group with respect to wild-type CATPO.

The most obvious change in the structure of the H82N is the presence of haem *b*, as suggested by spectral analysis (Fig. 6). Substitution of the imidazole ring by an amide group increases the size of the cavity above the haem, whereby W1 moves towards the side chain of Asn82 to make a hydrogen bond. W1 is also hydrogen-bonded to a new water, WA, which is not observed in the wild-type enzyme. The propionate group from

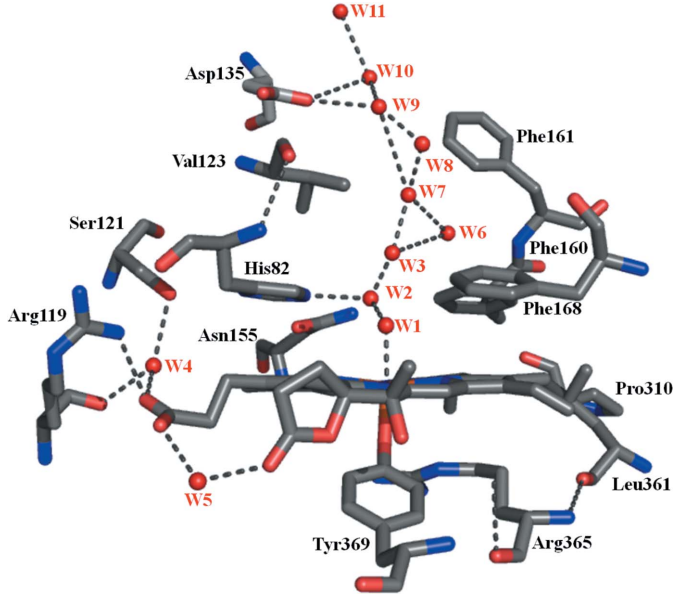

Figure 5
The haem environment of *S. thermophilum* CATPO. The catalytically important residues His82, Asn155, Ser121 and Val123 on the haem distal side are shown. Also displayed are the conserved residues lining the channel: Arg119, Asp135, Phe160, Phe161 and Phe168. The image shows the conserved residues Pro310, Leu361, Arg365 and Tyr369 on the proximal side. Hydrogen bonds are shown as dashed lines.

[1] Supplementary material has been deposited in the IUCr electronic archive (Reference: BE5222). Services for accessing this material are described at the back of the journal.

ring III of the unmodified haem *b* is hydrogen-bonded to the nearby Gln373 and Arg376 residues, which also interact with the adjacent W5.

Changing Val123 to the bulky side chain of phenylalanine reduces the size of the distal cavity, displacing several water molecules as it interposes between W2 and W10 and breaking the hydrogen bond to His82. Purified V123F exhibited low catalytic activity, consistent with interference of the larger side chain with substrate access to the active site. The structure also confirms that conversion from haem *b* to haem *d* has occurred.

4. Discussion

We have developed a recombinant expression system that allows the efficient intracellular production of CATPO in *E. coli*. The UV–Vis spectrum of recombinant CATPO exhibited absorption maxima similar to native CATPO and to *E. coli* HPII catalase, which indicated the presence of haem *d* (Loewen *et al.*, 1993). Haem *d*-containing catalases contain a high-spin ferric [iron(III)] system five-coordinate iron centre consisting of the porphyrin ring and a proximal tyrosine coordinated from the polypeptide. The observed CATPO absorbance bands at approximately 590 and 708 nm are indicative of high-spin iron(III) species. The spectral data for both the recombinant wild-type and the H82N and V123F variants, normalized to the main Soret absorption peak at 406 nm, revealed that the recombinant enzymes exhibit a Soret band ratio (A_{406}/A_{280} = 0.8–0.9) indicative of a higher haem content than in the native enzyme (A_{402}/A_{280} = 0.5). Thus, native CATPO seems to be deficient in haem *d*, perhaps having only approximately two moles of haem *d* per mole of tetramer. Surprisingly, given the low haem content of the purified native CATPO, the *B* factors for the haem in the native structure are similar to those of the surrounding protein, suggesting that the haem is present at full occupancy in the crystals. It is possible that a modification to the haem such as a cross-link might result in a perturbation of its spectral properties, as has been reported for the I274C mutant of KatE, which contains a Cys–haem cross-link (Jha *et al.*, 2012). However, there is no evidence for any covalent modification of the haem in the native CATPO structure.

A more likely hypothesis to explain the apparent discrepancy between the low haem content in solution and the full occupancy in the crystal is that crystallization preferentially selects the haem-containing form. The structure of a recombinant catalase depleted in iron has been reported (Andreoletti *et al.*, 2003), suggesting that catalase can fold in the absence of iron as long as the porphyrin is present. Interestingly, in this case crystallization also appeared to preferentially select the mature haem-containing protein, as the iron occupancy in the structure was refined to 60%, whereas the mature haem content measured using pyridine haemochromogen was only ∼30%. The most likely scenario here therefore appears to be that the purified native CATPO is somewhat deficient in haem content, resulting in a low Rz value, but that crystallization selects out the haem-containing, and possibly more stable, CATPO.

When this enzyme was first isolated, it was identified that the production of active CATPO was enhanced by the addition of copper, suggesting that the catalase and phenol oxidase activities may occur at distinct sites: a haem and a copper centre, respectively (Ögel *et al.*, 2006). We see no evidence in the crystal structure for any nonhaem prosthetic group. In order to test whether the haem group is indeed the redox centre for both the catalase and phenol oxidase activities, we investigated two active-site mutations. In other monofunctional catalases these mutations have been shown to affect H_2O_2 binding and the type of haem incorporated (Loewen *et al.*, 1993; Melik-Adamyan *et al.*, 2001; Chelikani *et al.*, 2003).

In the V123F variant, which contains haem *d*, the larger phenyl side chain was introduced to reduce the size of the substrate-binding channel. As expected, this results in a

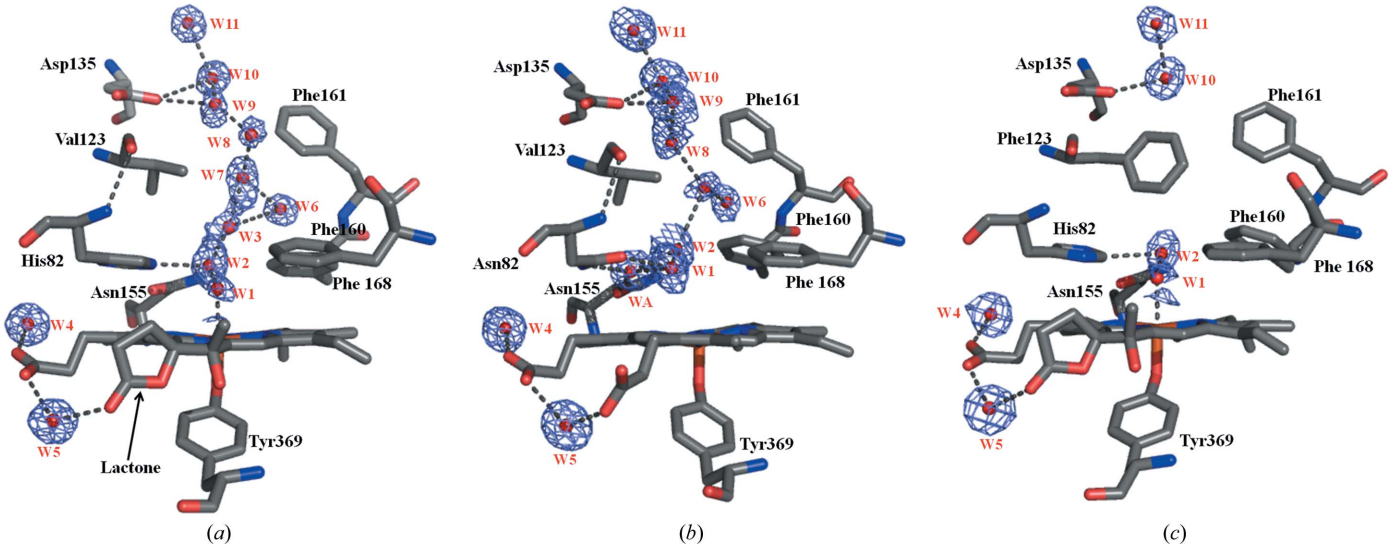

Figure 6
Water distribution in the main channel of *r*CATPO (*a*), the H82N variant (*b*) and the V123F variant (*c*). The $2F_o - F_c$ electron density corresponding to the individual water molecules is drawn at 1 r.m.s. and shown as a blue wire mesh.

marked reduction in catalase activity (0.3%). This variant also shows reduced phenol oxidase (10%) activity. The V123F mutation potentially acts in two ways. It probably sterically hinders the access of peroxide or oxygen to the active site and reduces the polarity of the active site owing to the displacement of waters, resulting in a less favourable environment for activated oxygen species. A second mutation, that of the conserved histidine (His82) to asparagine, has also been reported to perturb the haem active site by preventing the conversion of haem *b* to haem *d* (Loewen *et al.*, 1993). As expected, in this study the H82N variant contained haem *b* and displayed very low catalase activity (0.02%). In this case, dioxygen access to the active site is unhindered; however, the shorter asparagine side chain is presumably less able to steer productive binding and activation. This may alter the relative efficiencies of the catalase and oxidase activities and be reflected in a less marked effect on phenol oxidase activity (23%).

These data are consistent with the haem group acting as the redox centre in both the catalase and phenol oxidase activities. However, while both mutations severely affect the catalase activity, appreciable oxidase activity remains. This suggests that the binding site for oxidase substrates is not directly at the haem but is rather, as previously proposed, at a site linked to the haem by an electron-transfer pathway (Sicking *et al.*, 2008; Olson & Bruice, 1995). In mammalian NADP(H)-binding catalases, the NADPH, which binds in a pocket >10 Å away from the haem, has been proposed to either prevent formation of the inactive compound II or to reduce compound I under low-H_2O_2 conditions to reduce the risk of damage to the catalase active site (Kirkman & Gaetani, 2007). It is possible that the PO activity fulfils a similar role, but at such a low rate that the higher haem content of the recombinant protein does not have a significant effect on the observed PO rate.

The structure of CATPO shows a high degree of structural similarity to previously determined catalase structures. This supports our previous work (Sutay Kocabas *et al.*, 2008) demonstrating that the catalase activity dominates in the presence of H_2O_2. However, in the absence of H_2O_2 there is clear evidence for a low level of phenol oxidase activity (Sutay Kocabas *et al.*, 2008), suggesting that *in vivo* phenolic substrates will be oxidized in the presence of oxygen. It is not possible at this stage to determine the biological significance of the phenol oxidase activity. This oxidase activity has also been shown to occur in other catalases. Vetrano *et al.* (2005) demonstrated oxidase activity in a range of mammalian catalases, including those from bovine and mouse liver and mouse and human keratinocytes and fibroblasts, as well as purified enzyme preparations. We have also demonstrated phenol oxidase activity in CATPO and in various commercially available catalase samples from human erythrocytes, bovine liver and *C. glutamicum*, as well as from another fungal source, *A. niger*. We speculate that this secondary oxidase activity may be a general feature of some, if not all, catalases, but that in most cases it has not been detected owing to its relatively low level and the fact that most work on these enzymes has focused on their primary catalase activity.

Our recombinant expression system and new structural models provide a sound basis for further structure-based studies to dissect further the two distinct catalytic activities of this bifunctional fungal enzyme. We anticipate that such studies will provide information that translates to a wide number of catalases from diverse sources. Bifunctionality may also provide some advantages for industrial applications such as detoxification and/or the action of chemoprotective agents, particularly if the oxidase activity can be enhanced through engineering or directed evolution.

We would like to thank the Middle East Technical University (BAP-08-11-DPT2002K120510), ÖYP-DPT, the Biotechnology and Biological Research Council for funding (MJM and SEVP) and TUBITAK (IPDRFP-2219). We are also grateful to Professor R. E. Sockett and Dr John Taylor (University of Nottingham) for providing vector pET28aTEV.

References

Alfonso-Prieto, M., Borovik, A., Carpena, X., Murshudov, G., Melik-Adamyan, W., Fita, I., Rovira, C. & Loewen, P. C. (2007). *J. Am. Chem. Soc.* **129**, 4193–4205.
Andreoletti, P., Sainz, G., Jaquinod, M., Gagnon, J. & Jouve, H. M. (2003). *Proteins*, **50**, 261–271.
Bendtsen, J. D., Nielsen, H., von Heijne, G. & Brunak, S. (2004). *J. Mol. Biol.* **340**, 783–795.
Bravo, J., Fita, I., Ferrer, J. C., Ens, W., Hillar, A., Switala, J. & Loewen, P. C. (1997). *Protein Sci.* **6**, 1016–1023.
Bravo, J., Maté, M. J., Schneider, T., Switala, J., Wilson, K., Loewen, P. C. & Fita, I. (1999). *Proteins*, **34**, 155–166.
Bravo, J., Verdaguer, N., Tormo, J., Betzel, C., Switala, J., Loewen, P. C. & Fita, I. (1995). *Structure*, **3**, 491–502.
Carpena, X., Soriano, M., Klotz, M. G., Duckworth, H. W., Donald, L. J., Melik-Adamyan, W., Fita, I. & Loewen, P. C. (2003). *Proteins*, **50**, 423–436.
Chelikani, P., Carpena, X., Fita, I. & Loewen, P. C. (2003). *J. Biol. Chem.* **278**, 31290–31296.
Chelikani, P., Fita, I. & Loewen, P. C. (2004). *Cell. Mol. Life Sci.* **61**, 192–208.
Chen, V. B., Arendall, W. B., Headd, J. J., Keedy, D. A., Immormino, R. M., Kapral, G. J., Murray, L. W., Richardson, J. S. & Richardson, D. C. (2010). *Acta Cryst.* D**66**, 12–21.
Díaz, A., Horjales, E., Rudiño-Piñera, E., Arreola, R. & Hansberg, W. (2004). *J. Mol. Biol.* **342**, 971–985.
Díaz, A., Loewen, P. C., Fita, I. & Carpena, X. (2012). *Arch. Biochem. Biophys.* **525**, 102–110.
Díaz, A., Muñoz-Clares, R. A., Rangel, P., Valdés, V. J. & Hansberg, W. (2005). *Biochimie*, **87**, 205–214.
Díaz, A., Valdés, V. J., Rudiño-Piñera, E., Horjales, E. & Hansberg, W. (2009). *J. Mol. Biol.* **386**, 218–232.
Emsley, P., Lohkamp, B., Scott, W. G. & Cowtan, K. (2010). *Acta Cryst.* D**66**, 486–501.
Engh, R. A. & Huber, R. (1991). *Acta Cryst.* A**47**, 392–400.
Evans, P. R. (1997). *Jnt CCP4/ESF–EACBM Newsl. Protein Crystallogr.* **33**, 22–24.
Evans, P. R. (2011). *Acta Cryst.* D**67**, 282–292.
Fita, I., Silva, A. M., Murthy, M. R. N. & Rossmann, M. G. (1986). *Acta Cryst.* B**42**, 497–515.
Goldberg, I. & Hochman, A. (1989). *Biochem. Biophys. Acta*, **991**, 330–336.
Gouet, P., Jouve, H. M. & Dideberg, O. (1995). *J. Mol. Biol.* **249**, 933–954.
Håkansson, K. O., Brugna, M. & Tasse, L. (2004). *Acta Cryst.* D**60**, 1374–1380.

Hara, I., Ichise, N., Kojima, K., Kondo, H., Ohgiya, S., Matsuyama, H. & Yumoto, I. (2007). *Biochemistry*, **46**, 11–22.
Jha, V., Chelikani, P., Carpena, X., Fita, I. & Loewen, P. C. (2012). *Arch. Biochem. Biophys.* **526**, 54–59.
Kabsch, W. (2010). *Acta Cryst.* D**66**, 125–132.
Kirkman, H. N. & Gaetani, G. F. (2007). *Trends Biochem. Sci.* **32**, 44–50.
Klotz, M. G. & Loewen, P. C. (2003). *Mol. Biol. Evol.* **20**, 1098–1112.
Ko, T.-P., Safo, M. K., Musayev, F. N., Di Salvo, M. L., Wang, C., Wu, S.-H. & Abraham, D. J. (2000). *Acta Cryst.* D**56**, 241–245.
Leslie, A. G. W. (1999). *Acta Cryst.* D**55**, 1696–1702.
Loewen, P. C., Carpena, X., Rovira, C., Ivancich, A., Perez-Luque, R., Haas, R., Odenbreit, S., Nicholls, P. & Fita, I. (2004). *Biochemistry*, **43**, 3089–3103.
Loewen, P. C., Switala, J., von Ossowski, I., Hillar, A., Christie, A., Tattrie, B. & Nicholls, P. (1993). *Biochemistry*, **32**, 10159–10164.
Maté, M. J., Murshudov, G., Bravo, J., Melik-Adamyan, W., Loewen, P. C. & Fita, I. (2001). *Encyclopedia of Inorganic and Bioinorganic Chemistry*, edited by R. A. Scott, pp. 486–502. New York: John Wiley & Sons.
Maté, M. J., Zamocky, M., Nykyri, L. M., Herzog, C., Alzari, P. M., Betzel, C., Koller, F. & Fita, I. (1999). *J. Mol. Biol.* **286**, 135–149.
Melik-Adamyan, W., Bravo, J., Carpena, X., Switala, J., Maté, M. J., Fita, I. & Loewen, P. C. (2001). *Proteins*, **44**, 270–281.
Merle, P. L., Sabourault, C., Richier, S., Allemand, D. & Furla, P. (2007). *Free Radic. Biol. Med.* **42**, 236–246.
Moyer, D. (1997). US Patent 5646025.
Murshudov, G. N., Grebenko, A. I., Barynin, V., Dauter, Z., Wilson, K. S., Vainshtein, B. K., Melik-Adamyan, W., Bravo, J., Ferrán, J. M., Ferrer, J. C., Switala, J., Loewen, P. C. & Fita, I. (1996). *J. Biol. Chem.* **271**, 8863–8868.
Murshudov, G. N., Melik-Adamyan, W. R., Grebenko, A. I., Barynin, V. V., Vagin, A. A., Vainshtein, B. K., Dauter, Z. & Wilson, K. S. (1992). *FEBS Lett.* **312**, 127–131.
Murshudov, G. N., Skubák, P., Lebedev, A. A., Pannu, N. S., Steiner, R. A., Nicholls, R. A., Winn, M. D., Long, F. & Vagin, A. A. (2011). *Acta Cryst.* D**67**, 355–367.
Murthy, M. R. N., Reid, T. J. III, Sicignano, A., Tanaka, N. & Rossmann, M. G. (1981). *J. Mol. Biol.* **152**, 465–499.
Nicholls, P., Fita, I. & Loewen, P. C. (2001). *Adv. Inorg. Chem.* **51**, 51–106.
Nielsen, H., Engelbrecht, J., Brunak, S. & von Heijne, G. (1997). *Protein Eng.* **10**, 1–6.
Obinger, C., Maj, M., Nicholls, P. & Loewen, P. (1997). *Arch. Biochem. Biophys.* **342**, 58–67.
Ögel, Z. B., Yüzügüllü, Y., Mete, S., Bakir, U., Kaptan, Y., Sutay, D. & Demir, A. S. (2006). *Appl. Microbiol. Biotechnol.* **71**, 853–862.
Olson, L. P. & Bruice, T. C. (1995). *Biochemistry*, **34**, 7335–7347.
Peña-Soler, E., Vega, M. C., Wilmanns, M. & Williams, C. (2011). *Acta Cryst.* D**67**, 690–698.
Putnam, C. D., Arvai, A. S., Bourne, Y. & Tainer, J. A. (2000). *J. Mol. Biol.* **296**, 295–309.
Riise, E. K., Lorentzen, M. S., Helland, R., Smalås, A. O., Leiros, H.-K. S. & Willassen, N. P. (2007). *Acta Cryst.* D**63**, 135–148.
Sevinc, M. S., Ens, W. & Loewen, P. C. (1995). *Eur. J. Biochem.* **230**, 127–132.
Sicking, W., Korth, H. G., de Groot, H. & Sustmann, R. (2008). *J. Am. Chem. Soc.* **130**, 7345–7356.
Sutay Kocabas, D., Bakir, U., Phillips, S. E. V., McPherson, M. J. & Ogel, Z. B. (2008). *Appl. Microbiol. Biotechnol.* **79**, 407–415.
Sutay Kocabas, D., Pearson, A. R., Phillips, S. E. V., Bakir, U., Ogel, Z. B., McPherson, M. J. & Trinh, C. H. (2009). *Acta Cryst.* F**65**, 486–488.
Switala, J. & Loewen, P. C. (2002). *Arch. Biochem. Biophys.* **401**, 145–154.
Timkovich, R. & Bondoc, L. L. (1990). *Adv. Biophys. Chem.* **1**, 203–247.
Vagin, A. & Teplyakov, A. (2010). *Acta Cryst.* D**66**, 22–25.
Vainshtein, B. K., Melik-Adamyan, W. R., Barynin, V. V., Vagin, A. A. & Grebenko, A. I. (1981). *Nature (London)*, **197**, 411–412.
Vainshtein, B. K., Melik-Adamyan, W. R., Barynin, V. V., Vagin, A. A., Grebenko, A. I., Borisov, V. V., Bartels, K. S., Fita, I. & Rossmann, M. G. (1986). *J. Mol. Biol.* **188**, 49–61.
Vetrano, A. M., Heck, D. E., Mariano, T. M., Mishin, V., Laskin, D. L. & Laskin, J. D. (2005). *J. Biol. Chem.* **280**, 35372–35381.
Winn, M. D. *et al.* (2011). *Acta Cryst.* D**67**, 235–242.
Zámocký, M. & Koller, F. (1999). *Prog. Biophys. Mol. Biol.* **72**, 19–66.